

Steady and Unsteady Plasma Wall Jets for Separation and Circulation Control

B. Göksel*

Electrofluid Systems, Berlin, Germany

D. Greenblatt†, I. Rechenberg‡, C.N. Nayeri§, and C.O. Paschereit**

Technical University Berlin, Berlin, Germany

An experimental investigation of separation and circulation control was carried out using corona discharge as well as dielectric barrier discharge actuators at typical micro air vehicle (MAV) Reynolds numbers. All actuators were calibrated by direct measurement and their limitations were assessed on the basis of conventional low Reynolds number active flow control data. Aerodynamic data from corona discharge and high frequency dielectric barrier discharge actuators highlighted their applicability at MAV-type Reynolds numbers. Modulating the dielectric barrier discharge actuators at frequencies corresponding to reduced frequencies of $O(1)$, resulted in significant improvements to $C_{l,max}$, which increased with decreasing Re . At the low end of the MAV Reynolds number range ($Re \sim 20,000$) modulation increased $C_{l,max}$ by more than a factor of 2 and typical low Re hysteresis was eliminated. Of particular interest from an applications perspective was that performance, measured here by $C_{l,max}$, was shown to increase with decreasing duty cycle, and hence power input. In fact, duty cycles of around 0.66% were sufficient for effective separation control, corresponding to power inputs on the order of 1.2 milliwatts per centimeter.

Nomenclature

A	=	planform area, $b \times c$
AR	=	aspect ratio
b	=	airfoil span length
C_l	=	sectional lift coefficient, l/qc
C_d	=	sectional drag coefficient, d/qc
C_μ	=	steady momentum coefficient, J/qc
$\langle C_\mu \rangle$	=	unsteady momentum coefficient, $\langle J \rangle / qc$
c	=	airfoil chord-length, cylinder diameter
F^+	=	reduced excitation frequency, fX/U_∞
f	=	separation control excitation frequency
f_c	=	carrier frequency (RF)
J	=	steady plasma-induced momentum, $\int_0^\infty \rho(U_j^2 - U^2) dy$
$\langle J \rangle$	=	unsteady plasma-induced momentum, $\int_0^\infty \rho(\tilde{u}_j^2 + \tilde{v}_j^2) dy$
q	=	free-stream dynamic pressure
Re	=	Reynolds number based on chord-length

*Project Manager, Electrofluid Systems, 1 Volta Street, D-13355 Berlin, Germany, AIAA Member,
Email: berkant.goeksel@electrofluidsystems.com

†Research Scientist, Hermann Foettinger Institute for Fluid Mechanics, 8 Mueller-Breslau Street, D-10623 Berlin, Germany, AIAA Senior Member.

‡Professor, Institute of Process Engineering, 71-74 Acker Street, D-13355 Berlin, Germany.

§Research Scientist, Hermann Foettinger Institute for Fluid Mechanics, 8 Mueller-Breslau Street, D-10623 Berlin, Germany.

**Professor, Hermann Foettinger Institute for Fluid Mechanics, 8 Mueller-Breslau Street, D-10623 Berlin, Germany, AIAA Member.

U, V	=	mean velocities in directions x, y
U_∞	=	free-stream velocity
U_J	=	steady plasma-induced velocity
\tilde{u}_J, \tilde{v}_J	=	unsteady plasma-induced velocities in directions x, y
X	=	distance from perturbation to airfoil trailing-edge
x, y	=	coordinates measured from airfoil leading-edge
α	=	angle of attack

I. Introduction

Achieving sustained flight of micro air vehicles (MAVs) bring significant challenges due to their small dimensions and low flight speeds.¹ For so-called mini air vehicles, that operate in the $100,000 < Re < 300,000$ range, efficient systems can be designed by managing boundary layer transition via tripping at multiple locations.² However, at Reynolds numbers routinely experienced by MAVs ($Re < 100,000$), conventional low-Reynolds-number airfoils perform poorly, or even generate no useful lift. Some of the best performing airfoils in this Re range are cambered flat plates and airfoils with a thickness to chord ratio (t/c) of approximately 5%.¹ MAVs are usually designed with surveillance, sensing or detection in mind. Hence, a typical MAV mission should include a “high speed dash” ($V \sim 65 \text{ km/h}$, 18 m/s) to or from a desired location with significant head or tail winds and low-speed loiter ($V \sim 30 \text{ km/h}$, 8.3 m/s) while maneuvering, descending and climbing.³ Mueller defines two MAV sizes, which we can call “large” ($b=15 \text{ cm}$, $M=90 \text{ g}$) and “small” ($b=8 \text{ cm}$, $M=30 \text{ g}$).¹

As the Reynolds number decreases below about 100,000, the changes in airfoil performance are significant and boundary layer tripping becomes continuously more difficult, and at $Re < 50,000$ the separated laminar shear layer does not transition within the dimensions of the airfoil.¹ Consequently, unconventional approaches have been pursued, such as ornithopters that are inspired by bird and insect flight. Active control methods are also pursued. For example, Greenblatt & Wygnanski investigated perturbing an airfoil leading-edge boundary layer via two-dimensional periodic excitation at $Re \approx 50,000$ and $30,000$.⁸ Near-sinusoidal perturbations at $F^+ \approx 1$ resulted in the restoration of conventional low-Reynolds-number lift and aerodynamic efficiency, while excitation-induced lift oscillations were small and hysteresis associated with stall was eliminated. However, with decreasing Re larger periodic perturbations (expresses as $\langle C_\mu \rangle$) were required to generate useful lift. A similarity between the timescales associated with excitation and those characterizing dynamic stall in small flying creatures provided some insight into these observations. They observed that typical MAV dimensions are suited to actuation by means of micro-electromechanical systems (MEMS)-based devices. It was also noted that the effectiveness and efficiency of actuators required to supply the prescribed excitation will ultimately determine the success and limitations of the method.

Plasma-based actuators have recently demonstrated application to drag reduction and separation control.^{9-11,13-15,20} Separation control on airfoils at typical MAV Reynolds numbers ($10,000 < Re < 140,000$) were first demonstrated by plasma actuation using high voltage (10–20 kV) charged corona discharge wires in 1999.^{9,10} Göksel demonstrated significant improvement to an Eppler E338 airfoil performance [e.g. $C_{l,\max}$, $(l/d)_{\max}$], particularly for $10,000 < Re < 70,000$.⁹ For a given power input (in this case $\sim 8.5 \text{ Watts}$), $C_{l,\max}$ was shown to increase with decreasing Reynolds number up to 2.9 at $Re=10,000$. The reason for this is that the relative power input to the actuators, and presumed large relative momentum input, increased with decreasing Re . The relatively large power required to generate meaningful changes to aerodynamic indicators serves as a potential stumbling block in the way of plasma-based separation control. However, several comparisons of separation control by periodic excitation versus steady blowing have indicated that similar performance benefits (e.g. ΔC_l) can be achieved where $\langle C_\mu \rangle$ is up to two orders of magnitude smaller than C_μ . Using plasma actuators in a pulsed mode, Corke et al. have shown that steady forcing produced negligible changes to $C_{l,\max}$ while unsteady forcing at $F^+ = 1$ resulted in $\Delta C_{l,\max} \approx 0.2$ using only 2Watts.¹¹ Performance improvements using pulsed actuation were demonstrated on a delta wing using piezo-electric actuators by Margalit et al.,¹⁶ with maximum performance benefits occurring at $F^+ \approx 1$.

The global objective of the present investigation was to study separation and circulation control using plasma actuators at typical micro air vehicle Reynolds numbers (approximately $20,000 < Re < 80,000$). The first specific objective was to assess the performance and limitations of corona discharge wires from the perspective of separation and circulation control. This was done by analysing previously acquired airfoil data, described above, on the basis of calibrated actuator output (section II.A). The second objective was to study separation control employing a dielectric barrier discharge (DBD) actuator that was calibrated for both pulsed and non-pulsed actuation modes. Here a parametric study was carried out in order to establish the optimum reduced frequencies, minimum duty cycle and minimum power input. Optimization of the actuator’s design and placement were not considered.

II. Experimental Setup

For both actuator types considered here, calibration of the momentum generated was performed by direct measurements of the velocity profiles. The time independent (steady) momentum generated by the surface corona discharge method was measured using a flattened Pitot probe, while the steady and unsteady momentum components resulting from the DBD actuator were quantified via LDV measurements. Both actuators were calibrated in a closed-loop wind tunnel with a 2m long test section of 400 x 280mm in a quiescent environment ($U_\infty=0$) and at free-stream velocities corresponding to the Reynolds numbers employed here.

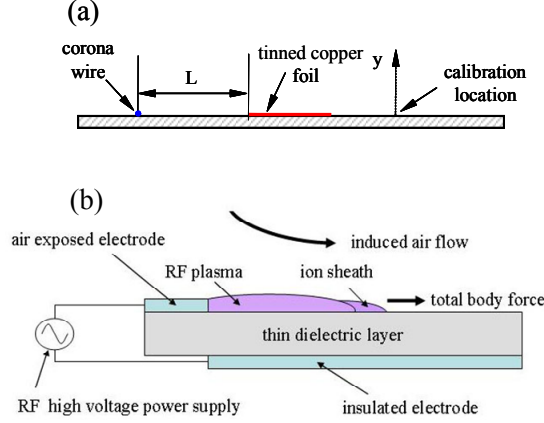


Fig. 1. Schematics of the calibrations setups used for (a) the corona discharge actuator and (b) DBD actuator.

A. Corona Discharge Actuator Calibration

Fig. 1a shows the setup for calibration of the surface corona discharge actuator. Various corona wire diameters (0.10mm and 0.15mm) and materials (copper and steel wires) were placed at various lengths upstream ($L=25\text{mm}$ to 45mm) of an earthed 25mm width tinned copper foil as shown in fig. 1a. The velocity profiles were measured 45mm downstream of the copper foil leading-edge. Typical velocity profiles for different wire diameters and wire types are shown in fig. 2a with conventional wall-jet scaling (U/U_∞ versus $y/y_{1/2}$) and profiles measured with a free stream present are shown in fig 2b. It was seen that the smaller diameter wire generated a higher momentum wall jet due to the smaller stronger local electric field strength (not shown). Also, the data for different wire diameters does not scale, but data for wire of the same diameter but different material does obey the scaling laws (fig. 2a). Peak velocity increased with decreasing L , but $L<25\text{mm}$ was not investigated due to the possibility of sparking. Based on the velocity profile measurements, the wall jet momentum was calculated according to

$$J = \int_0^\infty \rho(U_j^2 - U^2)dy, \quad (1)$$

where U is the time-mean velocity profile without plasma actuation (see fig. 2b).

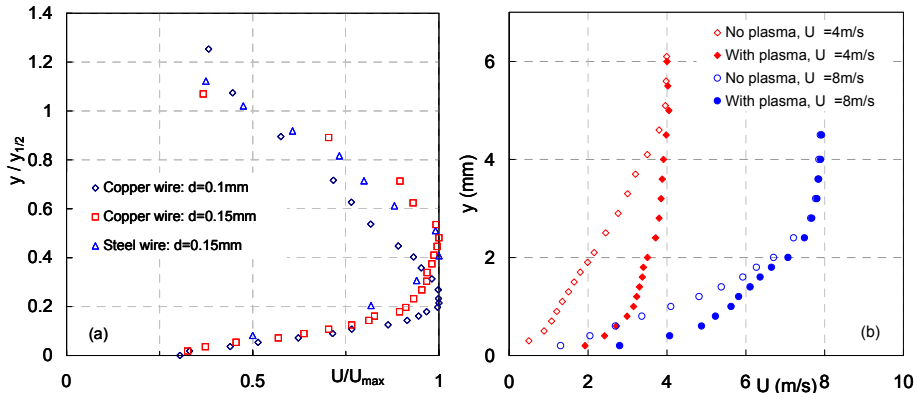


Fig. 2. Mean velocity profiles measured $x=45\text{mm}$ downstream of the copper foil leading-edge: (a) wall-jet scaling for different wire diameters and materials; velocity profiles with non-zero free stream velocities.

To estimate limits of applicability to boundary layer control, the conventional momentum coefficient defined for a two-dimensional control steady jet,¹⁷ namely

$$C_\mu = J / \frac{1}{2} \rho U_\infty^2 c \quad (2)$$

was calculated using the maximum momentum recorded (eqn. 1). By assuming typical MAV chord lengths, the results for C_μ versus Re are shown in fig. 3. The MAV range indicated in the figure is based on the definitions of “small” and “large” MAVs defined in ref. 1 above and assuming wing aspect ratios of $1 \leq AR \leq 2$, at the loiter target velocity. The approximate ranges of separation and circulation control, namely $C_{\mu,sep} \leq 4$ and $C_{\mu,circ} \geq 4$ respectively for $Re \sim 10^6$, are also shown on the figure.¹⁷ For conventional low Reynolds number flows, say $Re > 120,000$, the corona discharge wires used here are not capable of producing sufficient momentum to warrant application. In fact, even a two-fold increase in ionic wind velocities (i.e. a four-fold increase in C_μ) will only result in $C_\mu = 1\%$ at $Re = 200,000$ which would only produce modest boundary layer control. However, as we move down the Reynolds number scale we note a clear applicability of both separation and circulation control in the MAV Reynolds number range.

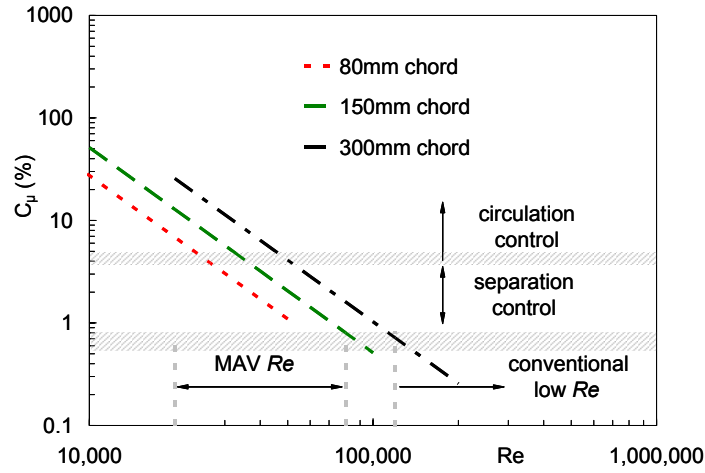


Fig. 3. Calibrated momentum coefficient based on direct measurement of the ionic wind wall jet for various values of chord length (c). MAV Re range is based on the definitions in ref. 1 and assumed $1 \leq AR \leq 2$ and loiter. Approximate ranges (hatched sections) of separation and circulation control at conventional low Re are from ref. 17.

B. Dielectric Barrier Discharge Actuator

The DBD actuator consists of two thin metal electrodes separated by a thin dielectric layer (fig. 1b).^{6,11-13} Sufficiently high voltages (at low radio frequencies in the kHz-range, denoted f_c) supplied to the actuator causes the air to weakly ionize at the edges of the upper electrodes. These are regions of high electric field potential. In this asymmetric configuration, the plasma is only generated at one edge (fig. 1b). The plasma moves to regions of increasing electric field gradients and induces a 2-D wall jet in the flow direction along the surface, thereby adding momentum to the boundary layer.⁶

Performing LDV profile measurements, at 3mm, 12mm and 25 mm downstream of the actuator, the steady momentum in the jet was quantified using eqn. 1. For the purpose of pulsed (or unsteady) actuation, the wave modulation method was employed where the kHz carrier wave at f_c is modulated by a square-wave that correspond to low frequencies appropriate (f) for separation control.^{11, 15-16} This introduces mean (U_j) and unsteady (\tilde{u}_j and \tilde{v}_j) velocity components and thus the jet momentum is made up of time-mean and oscillatory component quantified by

$$J_{tot} = J + \langle J \rangle = \int_0^\infty \rho (U_j^2 - U^2) dy + \int_0^\infty \rho (\tilde{u}_j^2 + \tilde{v}_j^2) dy, \quad (3)$$

where the first term represents the steady contribution (cf. eqn. 1) and the second term represents the oscillatory contribution. A similar exercise was performed for slot non-zero mass-flux slot blowing.¹⁹ For all data acquired here, the actuator was excited with a signal of intermittent bursts ($4.0 \text{ kHz} \leq f_c \leq 5 \text{ kHz}$) that were modulated in the range $2.5 \text{ Hz} \leq f \leq 100 \text{ Hz}$. The duty cycle was varied from $< 1\%$ to 100% at constant voltage. Consequently, the total momentum coefficient is defined as $C_{\mu,tot} = C_\mu + \langle C_\mu \rangle$ and also expressed as $(C_\mu, \langle C_\mu \rangle)$.¹⁹

LDV data for u and \tilde{u}_j at 3mm downstream of the actuator are shown for $U_\infty=0.83\text{m/s}$ and $U_\infty=5.79\text{m/s}$ in figs. 4a,b and 5a,b respectively. For all data acquired $\tilde{v}_j^2 \ll \tilde{u}_j^2$ could consequently be ignored without materially changing the results of eqn. 3. With no actuation (plasma off), a laminar Blasius boundary layer forms on the plate. At the lower velocity, jet actuation at all duty cycles considered here produces a significant steady and unsteady near wall momentum. In general, larger duty cycles produce larger near-wall mean-flow jets. On the other hand, driving the actuator in burst mode produces larger oscillatory components of momentum (table 1). Driving the actuator at 100% duty cycle produces a momentum deficit from approximately 2-3mm from the wall. This is believed to be a consequence of the vortical flow associated with the wall jet (fig. 4a). Also, a mild momentum surplus is generated for all actuator duty cycles in the outer part of the boundary layer. Note that no distinction has been drawn here between purely periodic perturbations and turbulent fluctuations, consequently \tilde{u}_j is representative of the overall unsteadiness.

As the free-stream velocity increases the relative momentum added to the flow decreases significantly. At $U_\infty=5.79\text{m/s}$ corresponding to $Re=70,000$, both steady and unsteady components of momentum are negligible (figs. 5a and 5b). Based on these data it is not expected that the plasma actuators will have a significant separation control effect for $Re>70,000$.

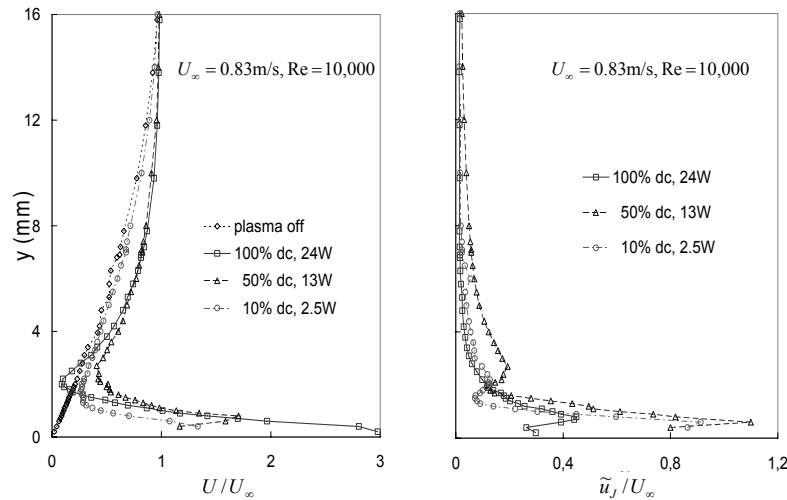


Fig. 4. Normalized mean velocity and turbulence intensity at the lowest finite free-stream velocity tested.

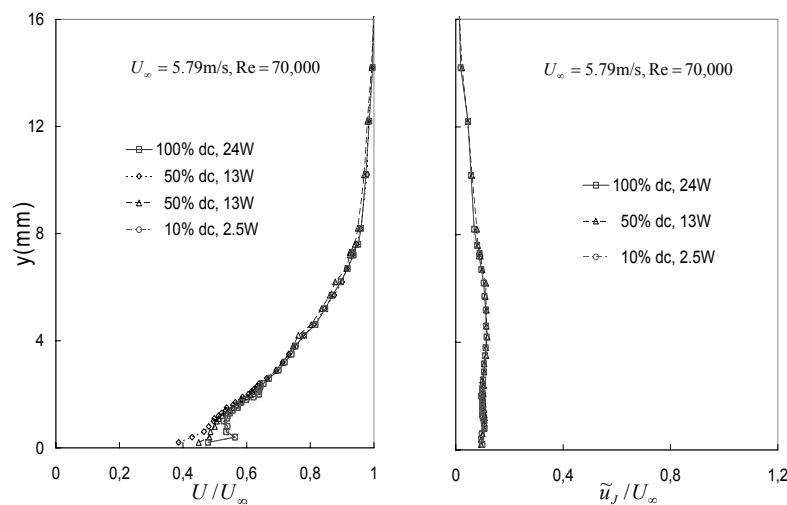


Fig. 5. Normalized mean velocity and turbulence intensity at an intermediate free-stream velocity.

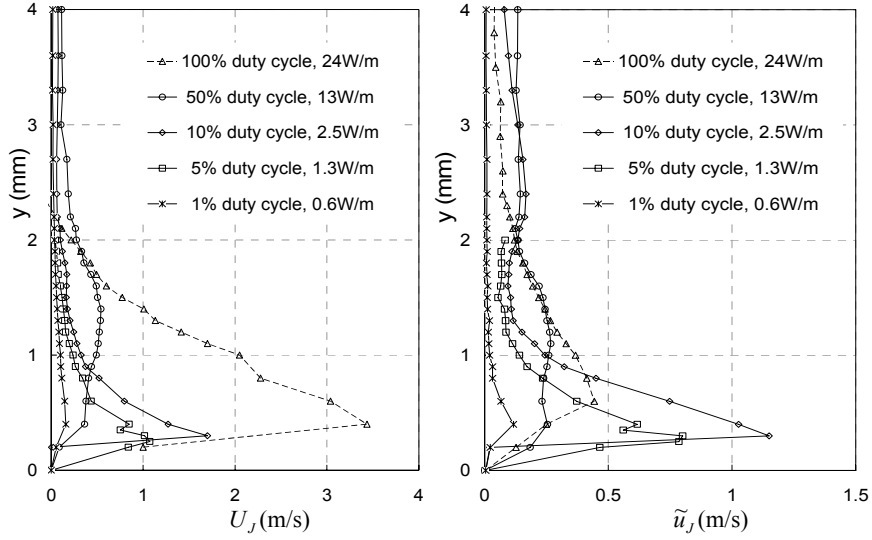


Fig. 6. Actuator calibration at 3mm downstream for different duty cycles at $U_\infty = 0$.

Fig. 6 shows actuator calibration data for $U_\infty=0$. In this case the duty cycle was gradually increased from 1% to 100%. It was noted that a duty cycle threshold between 2% and 4% is reached where there is a significant increase in near-wall unsteady momentum. Peak unsteady momentum is reached at a duty cycle of approximately 10%. Further increases in duty cycle result in decreases to both steady and unsteady near wall momentum. At 100% duty cycle a near-steady wall jet is formed with relatively large mean near wall momentum.

Table 1 Steady and unsteady actuator calibrations at various free stream velocities.

Duty Cycle (%)	C_u (%)	$\langle C_u \rangle$ (%)	U_∞ (m/s)
100	8.31	0.25	0.83
50	5.41	0.93	0.83
10	1.76	0.54	0.83
100	1.05	0.025	2.50
50	0.36	0.054	2.50
10	0.018	0.018	2.50
100	0.74	0.009	4.15
50	0.38	0.014	4.15
10	0.02	0.008	4.15

C. Airfoil Setup

Experiments were performed on an Eppler E338 airfoil (fig. 7a; $c=178\text{mm}$, $b=500\text{mm}$) and a circular cylinder (fig. 7a; $c=60\text{mm}$, $b=500\text{mm}$). Both were mounted between circular endplates and tested in two low speed open jet wind tunnels with 600mm and 1200mm diameter test sections respectively. Lift and drag were measured using a two component force balance. In the first set of experiments, the corona discharge actuators were placed in front of the airfoil and on the surface of the cylinder as shown in figs. 4a and 4b. All data were analyzed on the basis of the calibration described in section II.A above. In the second set of experiments the DBD actuator was placed on the upper surface of the airfoil at $x/c=1\%$. Airfoil performance was also assessed by tripping the boundary layer using a three-dimensional (3D) turbulator of height 200 microns and a two-dimensional (2D) step of height 100 microns, both at $x/c=1\%$. Maximum errors associated with C_l and C_d were ± 0.02 .

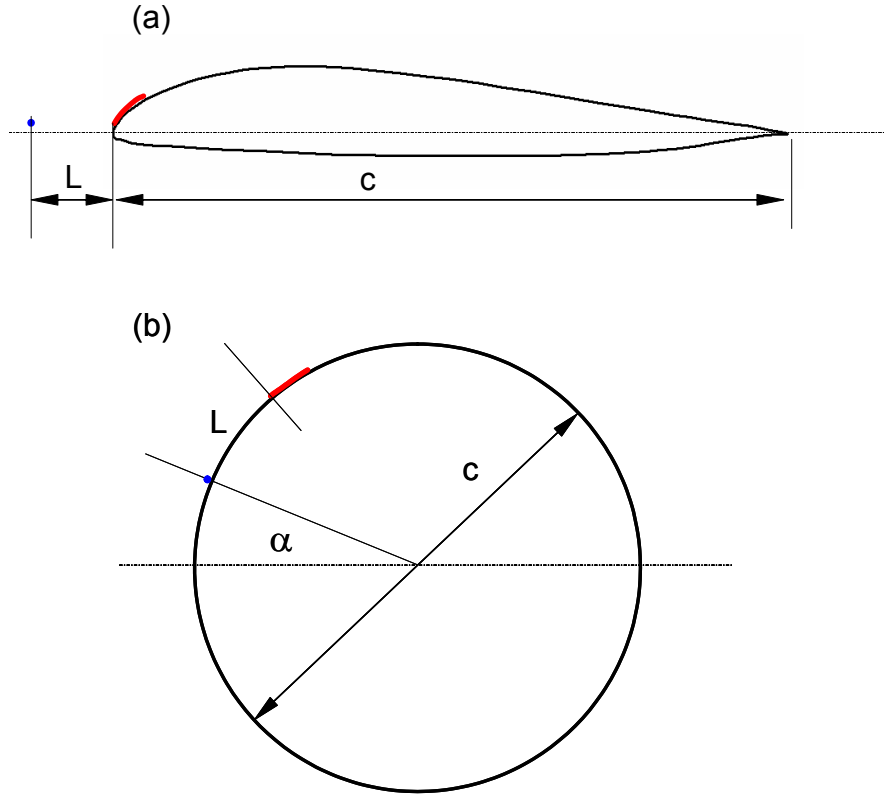


Fig. 7. Schematics of the (a) airfoil and (b) circular cylinder tested using the corona discharge actuator. The DBD actuator was tested on the airfoil by application at $x/c=1\%$ on the upper surface.

III. Discussion of Results

A. Corona Discharge Control

Separation control for $Re > 80,000$ had a negligible effect on $C_{l,max}$ for two reasons. Firstly, the airfoil performed relatively well, attaining 0.1 less than its conventional $C_{l,max}$ and secondly, $C_{\mu} < 0.5\%$, which is below the approximate threshold where steady separation control begins to show an effect. By decreasing the Reynolds number, and simultaneously increasing C_{μ} , the effect of the corona discharge on the aerodynamic coefficients C_l and C_d were evident as shown for $Re=65,000$ in figs. 8a,b. The airfoil performs poorly, but passive tripping of the boundary layer using a three-dimensional tabulator is effective at this Reynolds number, as shown by the increase in $C_{l,max}$. Tripping has the effect of almost restoring $C_{l,max}$ to typical conventional low Reynolds number value. With corona discharge control at this Reynolds number, $C_{\mu}=0.75\%$ corresponds to conventional separation control with a noticeable increase in $C_{l,max}$. Similar observations were made at $Re=39,600$ corresponding to $C_{\mu}=2.1\%$ (not shown). With successive decreases in Reynolds number the baseline airfoil can no longer generate useful lift as shown in figs. 9a and 9b. Control at these Reynolds numbers results in $C_{\mu} \geq 8.4\%$ which corresponds to conventional low Reynolds number circulation control, and the $C_{l,max}$ increase is significant. For $Re < 20,000$, at low angles of attack, thrust is generated and the lift curves become somewhat non-linear. $C_{l,max}$ data for the range $10,000 < Re < 140,000$ are summarized in fig. 11. Note that the log-scale does not clearly show that $dC_{l,max}/dC_{\mu}$ is greater for separation control than for circulation control. In addition, note that the present comparison is not typical because reductions in Re are being employed to effect an increase of C_{μ} .

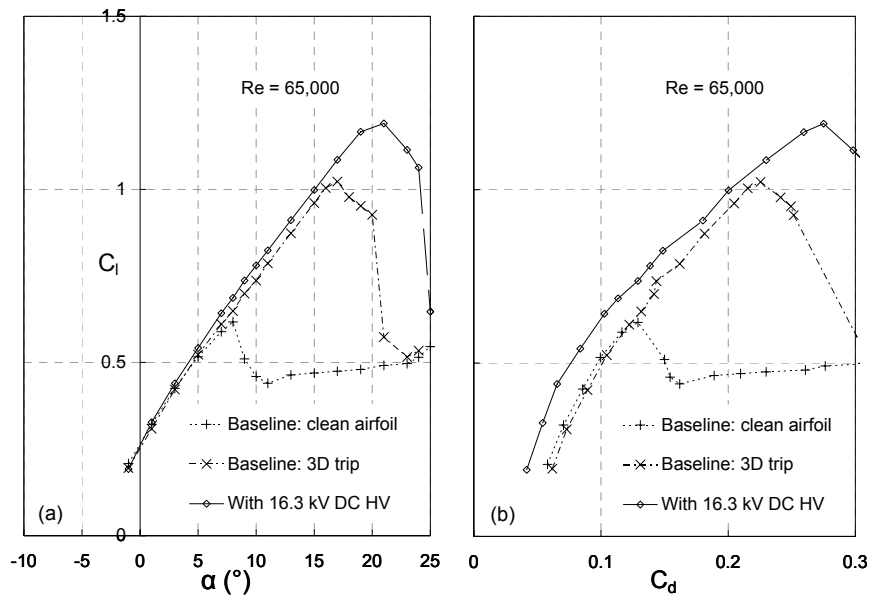


Fig. 8. Airfoil performance showing the effect of passive tripping and corona discharge corresponding to $C_{\mu}=0.75\%$.

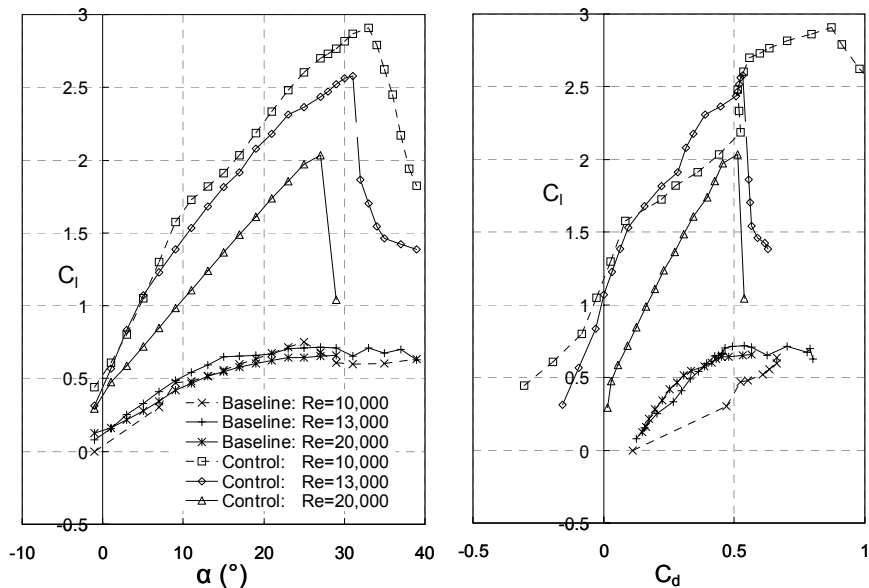


Fig. 9. Airfoil performance showing the effect of the corona discharge actuator where all control cases are at 8.5Watts (16.8 kV).

In a similar vein, for application of the corona discharge actuator to a circular cylinder (see schematic in fig. 7b), significant control authority was only attained at relatively small Re corresponding to large C_{μ} (see figs. 10 and 11). Maximum lift is attained when the corona wire is between 90° and 105° , where the angle corresponding to maximum lift appears to increase with decreasing Re . Nevertheless, all effective corona wire locations are downstream of the separation point which is typically $70^{\circ} < \alpha_s < 85^{\circ}$ at these Reynolds numbers. Based on inviscid theory, with $C_{l,max}=2.9$, the stagnation points on the cylinder are expected to lie 13° downwards from the horizontal plane through the cylinder diameter. Thus, the corona discharge is producing circulation control and is about $\frac{1}{4}$ of the C_l required to produce super-circulation. Based on extrapolation of the cylinder data in fig. 11, transition to super-circulation where the stagnation points merge at 90° downwards from the horizontal plane will occur at $C_{\mu} > 500\%$.

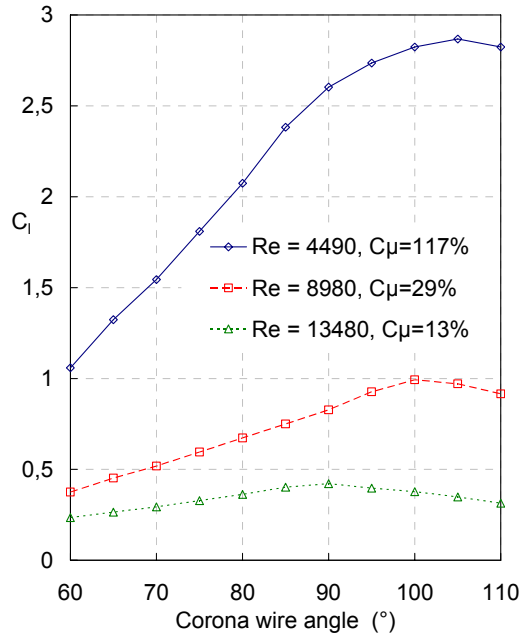


Fig. 10. Lift generated on a circular cylinder as a function of corona wire angle (see schematic in fig. 7b).

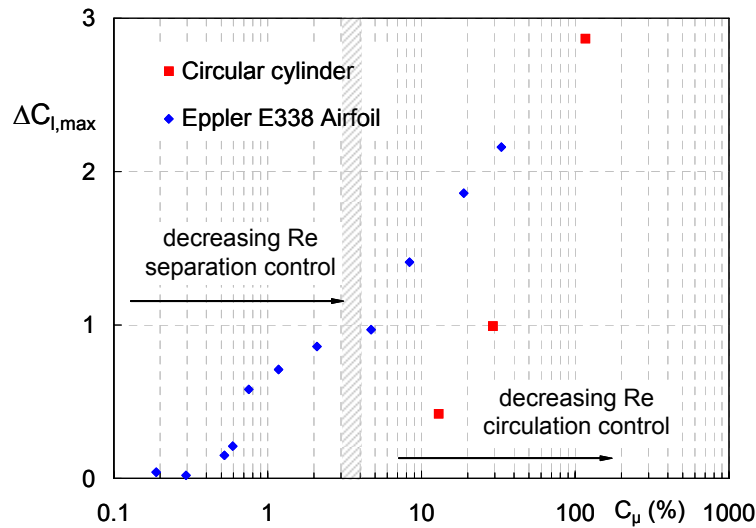


Fig. 11. Summary of maximum lift coefficient for the Eppeler E338 airfoil and the circular cylinder subject to corona discharge separation and circulation control. The hatched section demarcates the conventional low Reynolds number transition between separation control and circulation control.¹⁷

B. Dielectric Barrier Discharge Control

As in the previous section, airfoil data is presented in terms of decreasing Reynolds number, starting at conventional values ($Re \sim 140,000$) and successively reducing to $\sim 20,000$ (approximate lower MAV limit). We note that plasma control at 100% duty cycle has a *detrimental* effect and reduces $C_{l,max}$ (fig. 12). This is because a relatively low speed *effectively steady jet* being generated by the plasma actuator is markedly slower than in the free-stream velocity resulting in $C_\mu \approx 0.1\%$ (see section 2). This is not only below the threshold necessary for effective separation control; the low momentum fluid introduced near the wall, in fact, promotes separation. This may appear counterintuitive, but a similar effect was noted when using conventional steady slot blowing with $U_j/U_\infty < 1$.⁴

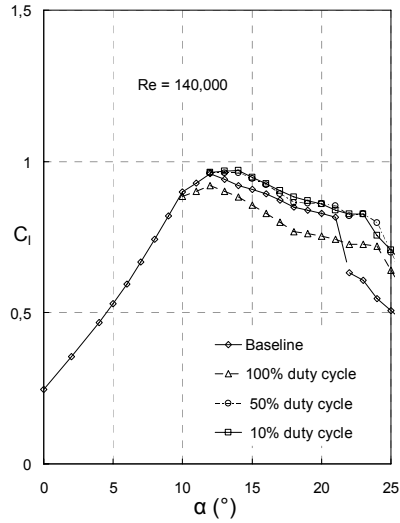


Fig. 12. Example of the effect of plasma actuation at $F^+=1$ on airfoil performance at conventional low Reynolds numbers.

All other duty cycles considered ($\leq 50\%$, corresponding to $F^+=1$) have a net positive post-stall effect with relatively low $\langle C_{\mu} \rangle < 0.1\%$. Changes to post-stall lift and small changes to $C_{l,max}$ at conventional low Reynolds numbers have been also observed by others.¹¹ Interestingly, data is marginally superior when the duty cycle is reduced from 50% to 10%. This might have been expected when considering the data in Fig. 6b, which shows that the 10% duty cycle actuation produced greater unsteady near-wall momentum. Moreover, this result is even more significant when we account for the fact that duty cycle percentage correlates linearly with power input.

With Reynolds number reduced to 80,000, the near wall jet velocity is comparable to that in the near wall boundary layer and the detrimental effect on $C_{l,max}$ disappears (not shown). At high post-stall angles, when the airfoil is fully stalled, the jet has a positive effect on C_l (not shown).

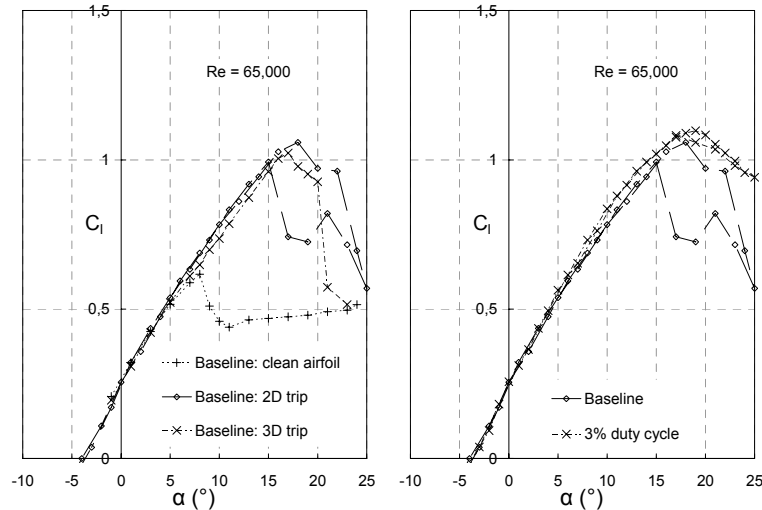


Fig. 13. Example of the effect of plasma actuation at $F^+=1$ on airfoil performance at Reynolds numbers $Re=65,000$.

At $Re=65,000$ the baseline clean airfoil performed poorly, but its performance improved with the addition of either 2D or 3D tripping (fig. 13a). 2D tripping was slightly superior, but the airfoil still suffered from significant hysteresis. In contrast, pulsed control at $F^+=1$ and 3% duty cycle virtually eliminating hysteresis and produced a slight increase in $C_{l,max}$.

At $Re=50,000$, also shown here for $F^+=1.0$, the effect of plasma actuation can be far more clearly observed (fig. 14a,b). As mentioned above,⁵ and shown in Figure 14a, it is virtually impossible to effectively promote transition passively at these Reynolds numbers, although the 2D trip was more effective than the 3D trip. This is reflected in the poor performance of the airfoil with $C_{l,max}<0.8$. For the purposes of presenting an unbiased evaluation, all DBD plasma actuation data presented in the remainder of this paper were compared with that of the 2D trip. In this instance, the 100% duty cycle actuation has a net positive effect on $C_{l,max}$ and this is because it generates a steady wall jet corresponding to $C_\mu=0.74\%$ (see table 1).

Successive reductions in duty cycle clearly result in improvements in performance, both with respect to the $C_l - \alpha$ linearity as well as $C_{l,max}$. Note, in addition, that $C_{l,max}$ is larger than that at the higher Reynolds numbers. It is assumed that this is due to the larger C_μ values which increase as a consequence of the reducing free-stream velocity. This runs counter to the typical baseline trends and has clear potential for reducing loiter speed discussed in the introduction.

Traditional steady separation is usually characterized by proportionality between performance indicators (e.g. $C_{l,max}$) and C_μ ,⁴ but this is not always the case when control is periodic.⁷ For the data present in fig. 14b, the conventional arguments of additional unsteady near wall momentum can be applied for duty cycles between 100% and 10% as discussed above. However, performance continues to improve as the duty cycle is reduced from 10% to 3% (fig. 14), despite the decreasing near wall momentum (cf. fig. 6). This is a perplexing phenomenon, but has practical ramifications when it is considered that power supplied to the actuators is proportional to duty cycle.

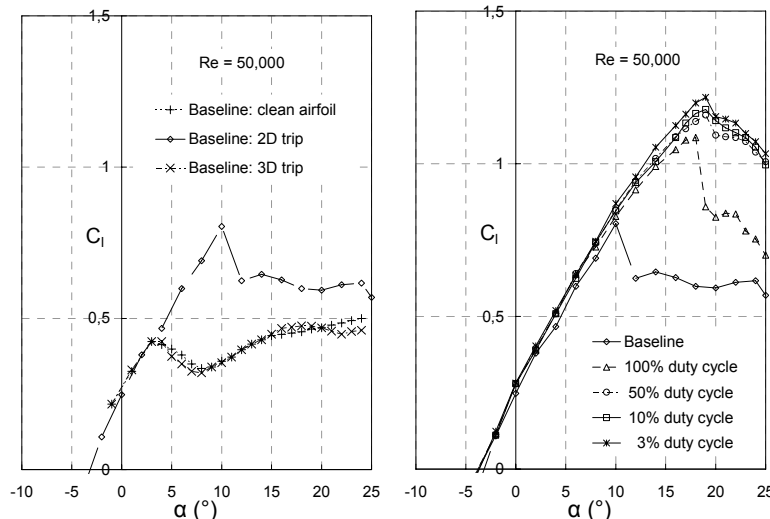


Fig. 14. Example of the effect of plasma actuation at $F^+=1$ on airfoil performance at Reynolds numbers $Re=50,000$.

Further reductions in Reynolds number to 35,000 and 20,500 showed ever greater effects on control. For example, in the latter case ($Re=20,500$) which is very near the low end of the MAV Reynolds number range, significant effects were observed and hence additional data were acquired in an attempt to optimize control. Employing a 5% duty cycle and placing the airfoil at a post stall angle of attack ($\alpha=18^\circ$) a frequency scan was performed for the range $0.25 \leq F^+ \leq 10.4$ (fig. 10). The optimum is seen to be at $F^+ \approx 1$ and this is consistent with conventional low Reynolds number data.⁷ Corke et al. observed that, using plasma actuators, the minimum voltage required to attach a post-stall separated flow was at $F^+ \approx 1$.¹¹

Similar effects have also been observed on delta wings using zero mass-flux jets.¹⁶ Further attempts at optimisation considered variation of the duty cycle. It was observed that the optimum lies somewhere between 3% and 8% (fig. 16), and this corresponds to the range where the maximum oscillatory momentum is added to the flow. However, the difference between the lift generated at optimum and non-optimum duty cycles differs by a small amount. This is significant because it means that similar performance benefits can be attained at a fraction of the power input. The effect of duty cycles is considered in more detail below.

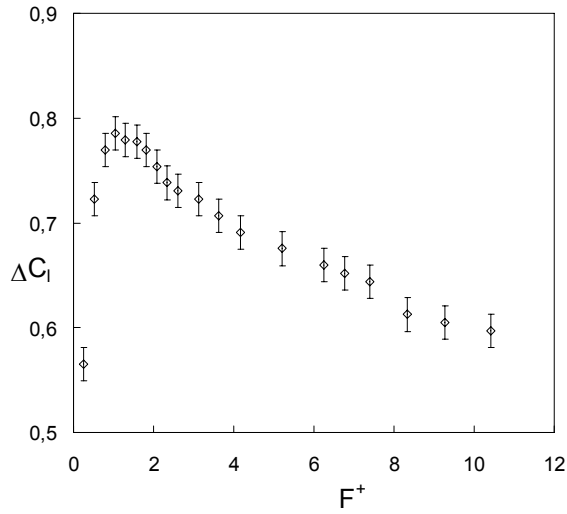


Fig. 15. Effect of reduced frequency on post-stall ($\alpha=18^\circ$) airfoil lift at $Re=20,500$; $\langle C_\mu \rangle \approx 0.05\%$ and duty cycle = 3%.

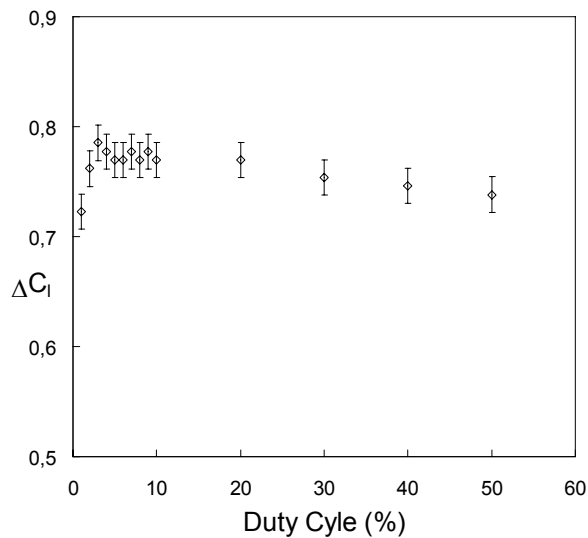


Fig. 16. Effect of duty cycle on post-stall ($\alpha=18^\circ$) airfoil lift at $Re=20,500$.

Further, the effect of input voltage on the C_l versus α curves was investigated. It was determined that for $V=10\text{kVpp}$ (corresponding to 5mW/cm ; $\langle C_\mu \rangle = 0.05\%$), the effect on the airfoil performance is clearly significant (fig. 17) and $C_{l,\text{max}}$ is larger than at higher Reynolds numbers (cf. fig. 12). Note that here the optimum F^+ and duty cycles have been used. Data was generated for increasing α (filled symbols) and decreasing α (open symbols). Note that below 10kVpp (8kVpp , corresponding to 4mW/cm ; $\langle C_\mu \rangle = 0.04\%$) the C_l versus α curve is highly non-linear where the airfoil appears to stall, but with increasing α begins once again to generate lift. This non-linear feature also has very little impact on $C_{l,\text{max}}$. It is of interest to note this non-linear feature does not show any significant hysteresis as the trend repeats for decreasing α (fig. 12). Similar observations were made by O'Meara and Mueller¹⁸ at $Re \sim 45,000$, who attributed the non-linear behavior to a separation bubble on the upper surface. Apparently, a longer bubble is associated with a decrease in the lift curve slope. It is not entirely clear here, however, how the bubble lengthens and then shortens in the presence of active control.

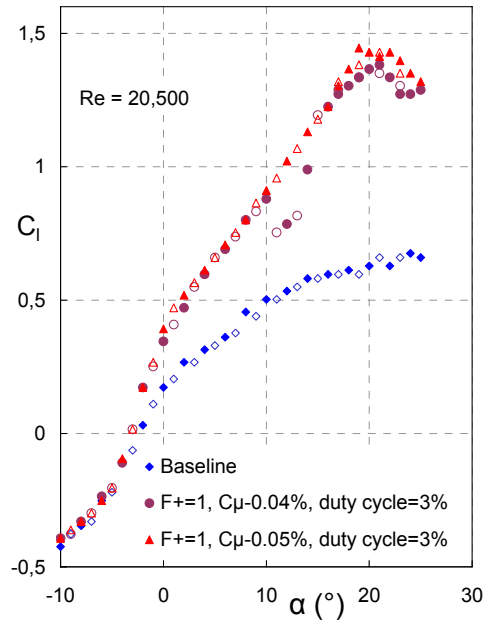


Fig. 17. Effect of plasma actuation on airfoil performance at a low MAV Reynolds number illustrating non-linear behavior at low power input and duty cycle = 3%).

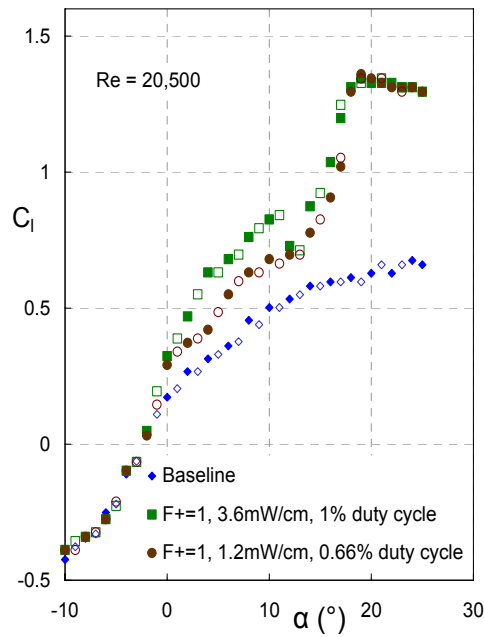


Fig. 18. Effect of plasma actuation on airfoil performance at a low MAV Reynolds number illustrating non-linear behavior at very low power input and duty cycles; $\langle C_\mu \rangle < 0.01\%$.

Finally, an effort was made to reduce the duty cycle even further while maintaining $C_{l,max}$. Fig. 18 shows results for 1% and 0.66% duty cycle. For these data the momentum input could not be reliably calibrated and the momentum coefficient $C_\mu < 0.01\%$. It was therefore deemed more meaningful to present the results in terms of milliwatts/cm as shown in fig. 18. It is clear that the lift slope remains highly non-linear, but at the lowest power input, namely 1.2mW/cm, there is no reduction in $C_{l,max}$. In fact, the lift slope now appears similar to the higher Reynolds number data of ref. 18.

IV. Conclusion

The present investigation considered separation and circulation control using corona discharge as well as separation control using steady and pulsed plasma actuation on an airfoil at typical MAV Reynolds numbers. All actuators were calibrated by direct measurement and their limitations were assessed on the basis of conventional low Reynolds number active flow control data. Airfoil and cylinder aerodynamic coefficient data acquired presently confirmed the applicability and limitations of the present actuators and, in particular, highlighted their applicability at MAV-type Reynolds numbers.

High frequency dielectric barrier discharge produced an effectively steady plasma wall jet and at times generated a loss of lift, where calibration indicated that again consistency with conventional lower Reynolds number active flow control. For example, steady, relatively low momentum steady actuation was detrimental at $Re > 100,000$, while beneficial at $Re = 50,000$ due to the four-fold increase relative momentum addition. Pulsing was achieved by modulating the high frequency plasma excitation voltage. The calibration indicated that variations of the duty cycle resulted in large differences between the steady and unsteady components of momentum addition.

Modulating the actuators at frequencies corresponding to $F^+ \approx 1$, resulted in improvements to $C_{l,max}$, which increased with reductions in Re . At the low end of the MAV Reynolds number range ($Re = 20,500$) modulation increased $C_{l,max}$ by more than a factor of 2. In addition, hysteresis associated with the baseline airfoil was eliminated. Of particular interest from an applications perspective was that performance, measured here by $C_{l,max}$, was shown to increase with decreasing duty cycle, and hence power input. In fact, duty cycles of around 0.66% were sufficient for effective separation control, corresponding to power inputs on the order of 1.2 milliwatts per centimeter.

Acknowledgments

We thank T. Schliwka and P. Albrecht for helping to calibrate the corona discharge actuators. We also acknowledge Y. Kastantin and Y. Singh for helping to calibrate the dielectric barrier discharge actuators using the two-component LDV system.

References

1. T.J. Mueller. "Aerodynamic Measurements at Low Reynolds Numbers for Fixed Wing Micro-Air Vehicles". Presented at the RTO AVT/VKI Special Course on Development and Operation of UAVs for Military and Civil Applications, VKI, Belgium, September 13-17, 1999.
2. A. Nagel, D.E. Levy and M. Shepshelovich, "Conceptual Aerodynamic Evaluation of MINI/MICRO UAV," AIAA Paper 2006-1261, 44th Aerospace Sciences Meeting and Exhibit, 9-12 January 2006, Reno, NV, 2006.
3. S.J. Morris. "Design and Flight Test Results for Micro-Signed Fixed-Wing and VTOL Aircraft". 1st International Conference on Emerging Technologies for Micro Air Vehicles, Georgia Institute of Technology, Atlanta Georgia, February 1997, pp. 117-131.
4. J.S. Attinello. "Design and Engineering Features of Flap Blowing Installations". In G.V. Lachmann. "Boundary Layer and Flow Control. Its Principles and Application", Volume 1, 1961, Pergamon Press, New York, pp. 463-515.
5. B.H. Carmichael. "Low Reynolds Number Airfoil Survey". NASA Contractor Report 165803, Volume I, November 1981.
6. J.R. Roth, D. Sherman and S. Wilkinson. "Boundary Layer Flow Control with One Atmosphere Uniform Glow Discharge Surface Plasma". AIAA 1998-0328, 1998.
7. D. Greenblatt and I. Wygnanski. "Control of separation by periodic excitation" In Progress in Aerospace Sciences, Volume 37, Issue 7, 2000, pp. 487-545.
8. D. Greenblatt and I. Wygnanski. "Use of Periodic Excitation to Enhance Airfoil Performance at Low Reynolds Numbers". In AIAA Journal of Aircraft, Volume 38, Issue 1, 2001, pp. 190-192.
9. B. Göksel. "Improvement of Aerodynamic Efficiency and Safety of Micro Aerial Vehicles by Separation Flow Control in Weakly Ionized Air". (in German) In Proceedings of the German Aerospace Congress, Leipzig, DGLR Paper JT-2000-203, 2000, pp. 1317-1331.
10. B. Göksel and I. Rechenberg. "Active Separation Flow Control Experiments in Weakly Ionized Air". In Andersson H. I. and Krogstad P.-Å. (eds.) Advances in Turbulence X, Proceedings of the 10th Euromech European Turbulence Conference, CIMNE, Barcelona, 2004.
11. T.C. Corke, C. He and M.P. Patel. "Plasma flaps and slats: An application of weakly ionized plasma actuators". AIAA Paper 2004-2127, 2nd AIAA Flow Control Conference, Portland, Oregon, 2004.
12. C.L. Enloe, T.E. McLaughlin, R.D. Van Dyken, K.D. Kachner, E. J. Jumper and T.C. Corke. "Mechanism and Responses of a Single Dielectric Barrier Plasma Actuator: Plasma Morphology". In AIAA Journal, Volume 42, Issue 3, 2004, pp. 589-594.
13. B. Göksel and I. Rechenberg. "Active Flow Control by Surface Smooth Plasma Actuators". In Rath H. J., Holze C., Heinemann H.-J., Henke, R. and Hönlinger H. (eds.) "New Results in Numerical and Experimental Fluid Mechanics V", Contributions to the 14th STAB/DGLR Symposium Bremen, Germany 2004, NNFM Vol. 92, Springer, 2006 (in press).

14. B. Göksel and I. Rechenberg “Experiments to Plasma Assisted Flow Control on Flying Wing Models”. Submitted for Proceedings of CEAS/KATnet Conference on Key Aerodynamic Technologies To Meet the Challenges of the European 2020 Vision, Bremen, 2005.
15. B. Göksel, D. Greenblatt, I. Rechenberg and C. O. Paschereit “Plasma Actuators for Active Flow Control”. DGLR Paper 2005-210, to be published in the Proceedings of the German Aerospace Congress 2006, Friedrichshafen, Germany, 2005.
16. S. Margalit, D. Greenblatt, A. Seifert and I. Wygnanski “Delta wing stall and roll control using segmented piezoelectric fluidic actuators”. In AIAA Journal of Aircraft, Volume 42, Issue 3, 2005, pp. 698-709.
17. Ph. Poisson-Quinton and L. Lepage “Survey of French research on the control of boundary layer and circulation”, in Lachmann, G. V., “Boundary layer and Flow Control. Its Principles and Application”, Volume 1, Pergamon Press, New York, 1961, pp. 21-73.
18. M.M. O'Meara and T.J. Mueller, “Laminar separation bubble characteristics on an airfoil at low Reynolds numbers,” AIAA Journal, Vol. 25, 1987, pp. 1033–1041.
19. A. Seifert, A. Darabi, and I. Wygnanski, “Delay of airfoil stall by periodic excitation”, AIAA Journal of Aircraft, Vol. 33, No. 4, 1996, pp. 691-698.
20. L. Léger, E. Moreau, and G. Touchard, “Electrohydrodynamic airflow control along a flat plate by a DC surface corona discharge – Velocity profile and wall measurements.” AIAA Paper 2002-2833. 1st AIAA Flow Control Conference, Missouri, 2002.